Systems & Control Transactions

Original Research Article
Peer Reviewed Conference Proceeding
ESCAPE 36 - European Symposium on Computer Aided Process Engineering
Sheffield, UK. 21-24 June 2026

PSE PRESS

Unveiling Reaction Patterns in Thermal and Catalytic Biomass Pyrolysis Using PCA and Multivariate Analysis

Martín Rodríguez-Fragoso[a], Sandro González-Arias[a], Octavio Elizalde-Solis[a], and Edgar Ramírez-Jiménez[a]*

[a] Department of Chemical Petroleum Engineering, ESIQIE, Instituto Politécnico Nacional, Mexico City, 07738, Mexico
* Corresponding Author: eramirezj@ipn.mx.

ABSTRACT

Understanding the relationships between operating conditions and product formation pathways in biomass pyrolysis remains challenging due to the complex interactions among temperature, catalytic effects, and feedstock composition. In this work, principal component analysis (PCA) was applied to investigate the combined influence of temperature and catalyst-to-biomass ratio on the pyrolysis of sugarcane bagasse and Salicornia. To preserve mechanistic interpretability, two complementary analyses were performed: one considering only catalytic experiments and a second integrating both thermal and catalytic conditions. Separate PCA were conducted for product yields, gas and liquid compositions, and solid-phase FTIR features. The results reveal that thermal conditions promote severe cracking and solid carbonization, whereas catalytic operation favors secondary pathways associated with controlled dehydration and partial stabilization of liquid products. Distinct patterns between the two feedstocks were also identified, reflecting their intrinsic compositional differences. Based on the multivariate trends identified, a conceptual reaction scheme is proposed to describe the interplay between thermal and catalytic pathways.

Keywords: Biomass, Multivariate Statistics, Reaction, Reaction Patterns

INTRODUCTION

Biomass pyrolysis is a promising thermochemical route to produce biofuels, value-added chemicals, and carbonaceous materials from renewable resources. Lignocellulosic biomass, due to its abundance and carbon-neutral nature, has attracted significant attention as a feedstock for sustainable energy systems. Nevertheless, the intrinsic complexity of biomass and the large number of simultaneous reactions occurring during thermal conversion hinder a detailed understanding of the reaction mechanisms and the control of product distribution [1-2].

From a mechanistic standpoint, biomass pyrolysis is generally described as the superposition of three main primary pathways: char formation, depolymerization, and fragmentation of the macromolecular constituents. These reactions are accompanied by secondary processes such as cracking, recombination, and recondensation of volatile species, which may lead to the formation of low- and high-molecular-weight products as well as secondary char. The relative contribution of these pathways strongly depends on temperature and reactor conditions, resulting in a highly interconnected and nonlinear reaction network [1-2].

The pyrolysis behavior of lignocellulosic biomass is governed by the relative proportions and interactions of cellulose, hemicellulose, and lignin. However, several studies have shown that the pyrolysis of whole biomass cannot be accurately described as a simple superposition of its individual components. Interactions among the main constituents significantly affect product yields and reaction pathways, and their detailed mechanisms remain not fully understood [3].

As an alternative, data-driven methodologies have gained increasing attention for the analysis of complex pyrolysis datasets. Principal Component Analysis (PCA) has been successfully employed to identify dominant patterns, correlate product families, and distinguish between primary and secondary reactions, supporting the proposal of reaction or kinetic schemes without imposing *a priori* assumptions [4].

In this work, an integrated PCA-based approach is

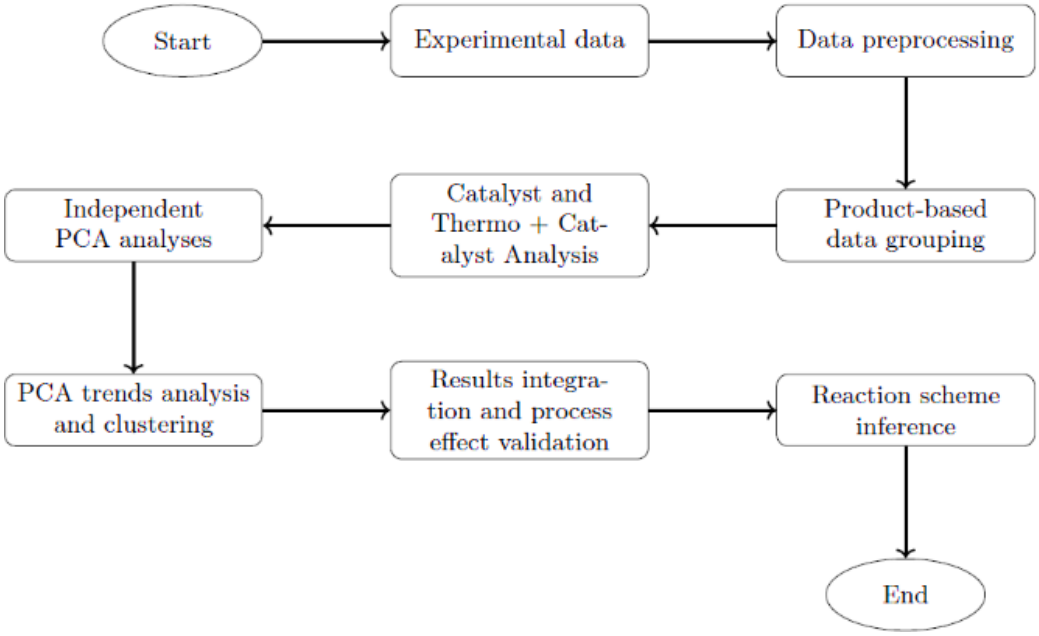

Figure 1. Flowchart of PCA methodology.

applied to investigate the catalytic and thermal pyrolysis of lignocellulosic biomass by combining complementary experimental data sets, including global product yields, gas chromatography, and FTIR analysis of solid residues. Independent PCA analyses are performed and subsequently interpreted as a function of temperature and C/B ratio, together with clustering techniques to identify distinct reaction regimes.

EXPERIMENTAL SETUP

Two biomasses were investigated: sugarcane bagasse and Salicornia sp. Sugarcane bagasse (SCB) was obtained from the Tierra Blanca Sugar Mill (Veracruz, Mexico), while Salicornia (SAA) was collected from cultivated fields in Baja California Sur, Mexico. Both materials were used as feedstock for thermal and catalytic pyrolysis experiments.

Pyrolysis reactions were carried out in a semi-continuous fixed-bed tubular reactor made of titanium, using 1 g of biomass per experiment. Thermal pyrolysis was conducted in the absence of catalyst, whereas catalytic pyrolysis experiments were performed using catalyst-to-biomass (C/B) mass ratios of 1:1, 1:2, and 1:3. For both biomasses, experiments were conducted at reaction temperatures ranging from 400 to 600 °C, while the residence time was kept constant. Nitrogen was continuously fed from the bottom of the reactor to ensure an inert atmosphere.

The experimental setup consisted of a heating furnace, the tubular reactor, a condensation column with a recirculating cooling system, a round-bottom flask for liquid recovery, and a gas collection system. Condensable volatiles were recovered using ethylene glycol as cooling medium at 5 °C, while non-condensable gases were collected in inert multilayer foil sampling bags.

The experimental campaign generated four types of data: (i) overall product yields, (ii) gas-phase composition determined by gas chromatography, (iii) liquid-phase composition analyzed by gas chromatography, and (iv) solid-phase FTIR spectra. Gaseous products were analyzed using a GC-7890B gas chromatograph equipped with a Molecular Sieve 13X column and argon as carrier gas. Liquid products were analyzed using a Clarus 500 gas chromatograph. Solid residues were characterized by FTIR spectroscopy using a PerkinElmer Precisely Spectrum 100 spectrometer.

METHODOLOGY

The methodology implemented in this work follows a product-based multivariate analysis strategy, as summarized in Fig. 1. The approach integrates experimental data from different product phases with structured data preprocessing and Principal Component Analysis (PCA) to identify dominant trends and infer reaction pathways during biomass pyrolysis.

Data Preprocessing

All data processing was performed using `Python`, employing standard scientific libraries (`NumPy`, `Pandas`, and `scikit-learn`)[5-7].

Overall product yields, gas-phase compositions, liquid-phase grouped variables, and solid-phase FTIR

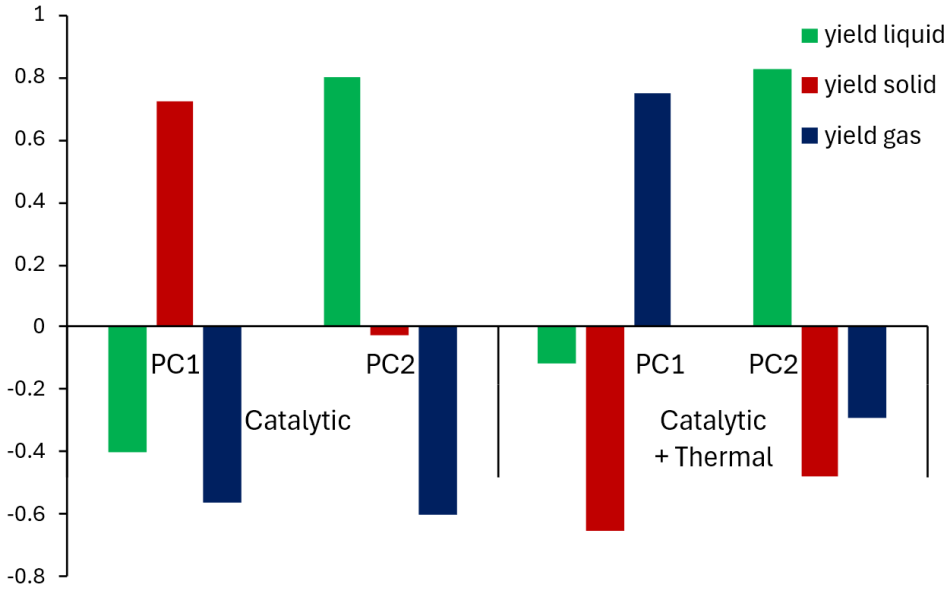

Figure 2. Bar plots of yield loadings for each data group.

descriptors were scaled using z-score normalization to ensure comparable variable variance prior to multivariate analysis.

Gas-phase data consisted of the molar fractions of the main species (CH_4, CO_2, C_2H_6, C_3H_8, C_4H_{10}, H_2, and CO), which were directly used as input variables. Liquid-phase chromatographic data were first grouped into chemical families (alcohols, ketones, methylphenols, nitrophenols, and chlorophenols) to reduce dimensionality and improve chemical interpretability.

For solid-phase analysis, FTIR spectra were divided into predefined wavenumber intervals (2700–2350, 2350–2100, 2100–1800, 1800–1500, and 1300–850 cm^{-1}). The area under each interval was calculated using numerical integration, providing quantitative descriptors associated with major functional groups in the solid residues.

Product-based PCA strategy

PCA was applied independently to each product-based dataset using the `scikit-learn` implementation. In all cases, the first two principal components were retained, as they captured the dominant variance and allowed visualization of process trends. To enhance discrimination of reaction regimes, the data were separated into two subsets: catalytic-only and combined thermal–catalytic experiments. Independent PCA models were constructed for each subset, the analysis resulted in a total of eight PCA models: four corresponding to catalytic experiments and four corresponding to the thermal–catalytic dataset.

For each model, the loading patterns of PC1 and PC2 were analyzed to assign physical and chemical meaning to the principal components, while score plots were used to evaluate the evolution of these behaviors as a function of temperature, C/B ratio, and biomass type. Clustering in the score space was further assessed using the `KMeans` algorithm to identify groups exhibiting similar process behavior.

RESULTS AND DISCUSSION

Table 1 summarizes the explained variance of the first two principal components for yields, gas, liquid, and solid (FTIR) datasets under catalytic and combined catalytic–thermal conditions.

Table 1: Explained Variance for each PCA analysis.

	Explained Variance			
	Catalytic		Catalytic + Thermal	
	PC1	PC2	PC1	PC2
Yields	0.639	0.361	0.523	0.477
Gas	0.331	0.237	0.331	0.237
Liquid	0.480	0.303	0.492	0.317
Solid FTIR	0.800	0.175	0.747	0.227

For product yields, the catalytic system is predominantly described by PC1, indicating a dominant reaction pathway. When thermal experiments are included, the variance is more evenly distributed between PC1 and PC2, revealing the coexistence of temperature-driven and catalyst-assisted mechanisms.

Gas-phase data display a similar variance

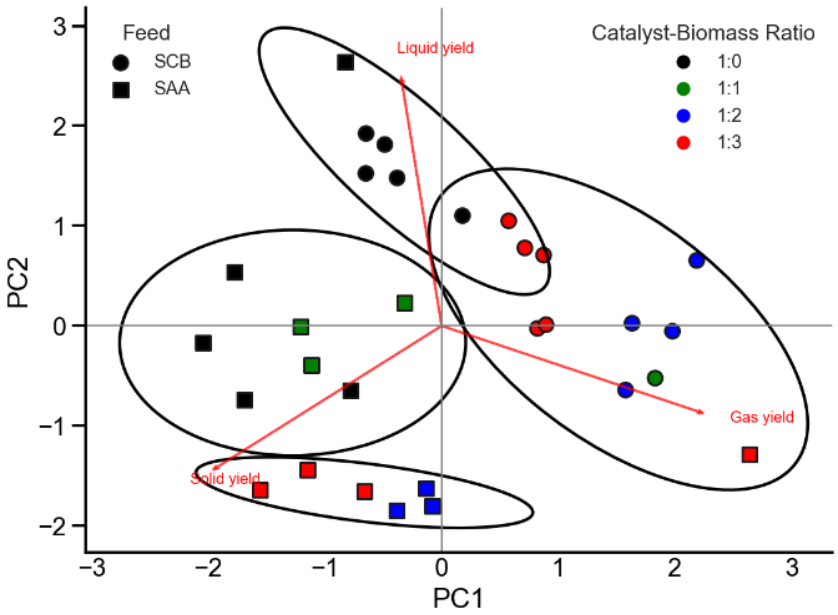

Figure 3. Biplot of thermal + catalytic yields scores.

distribution in both cases, suggesting that gas formation is primarily governed by temperature, with limited sensitivity to catalytic effects. In contrast, liquid-phase data show a more balanced contribution of PC1 and PC2, reflecting the superposition of thermal fragmentation and catalytic stabilization pathways. Solid residues characterized by FTIR are largely dominated by PC1 in both scenarios, indicating a robust primary mechanism associated with char formation and structural evolution. The increased contribution of PC2 upon inclusion of thermal experiments suggests secondary temperature-induced modifications without altering the dominant catalytic signature.

PCA of Product Yields

Loading Analysis

The loadings bar plots for product yields (see Fig. 2) highlight clear differences between the PCA performed using only catalytic experiments and the one including both catalytic and thermal conditions.

For the catalytic dataset, PC1 accounts for most of the variance and reflects the overall redistribution of products driven by secondary catalytic reactions, separating gas-dominated regimes from those favoring liquids and solids. This indicates that, in the presence of a catalyst, product yields are mainly controlled by the efficiency of catalytic cracking, dehydration, and aromatization pathways.

PC2 captures a secondary contrast associated with the balance between liquid stabilization and solid residue formation, characteristic of intermediate catalytic severities.

When thermal experiments are included, the variance structure becomes more evenly distributed between PC1 and PC2. This redistribution indicates that an additional, non-catalytic source of variability is introduced. In this case, PC1 represents a more general conversion severity axis, combining both catalytic effects and temperature-driven primary decomposition. PC2 gains importance as a discriminator between thermally dominated pathways, characterized by early gas formation and poor liquid stabilization, and catalytically assisted regimes, where yields are redistributed toward upgraded liquids and structured solids.

Biplot Analysis

Figs. 3 and 4 shows the PCA biplots of product yields for thermo-catalytic and purely catalytic experiments, with samples colored according to the C/B ratio. These biplots allow visualization of the combined effect of reaction regime and catalyst loading on the distribution of products.

For the thermo-catalytic experiments, most SCB samples are in the (+PC1, +PC2) region, while thermal bagasse experiments tend to shift toward the (−PC1, +PC2) quadrant. In contrast, SAA samples predominantly occupy the (−PC1, −PC2) region, with some thermo-catalytic conditions extending toward (−PC1, +PC2). A consistent downward trend along PC2 is observed with increasing C/B ratio for SAA, whereas for SCB the effect of C/B is more pronounced along PC1, with lower PC1 scores associated with lower catalyst loadings.

When considering only catalytic experiments (see

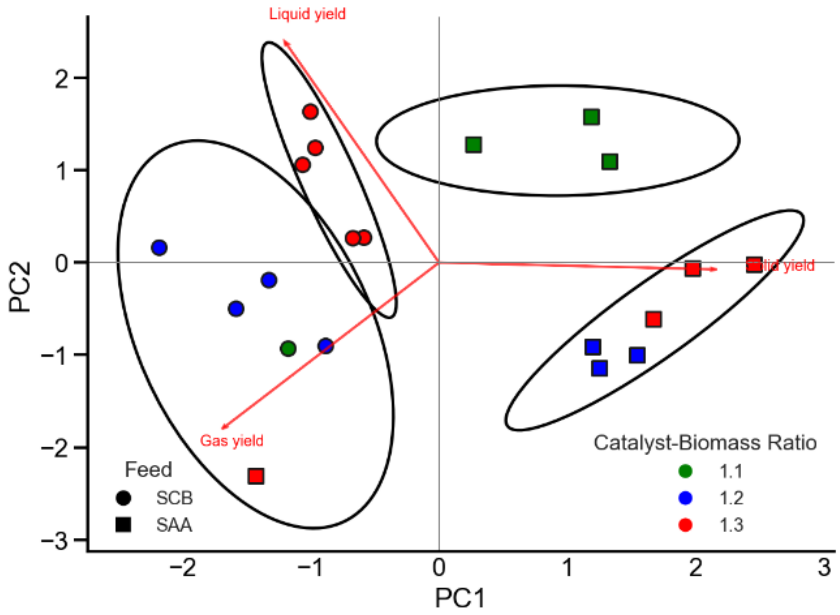

Figure 4. Biplot of only catalytic yields scores.

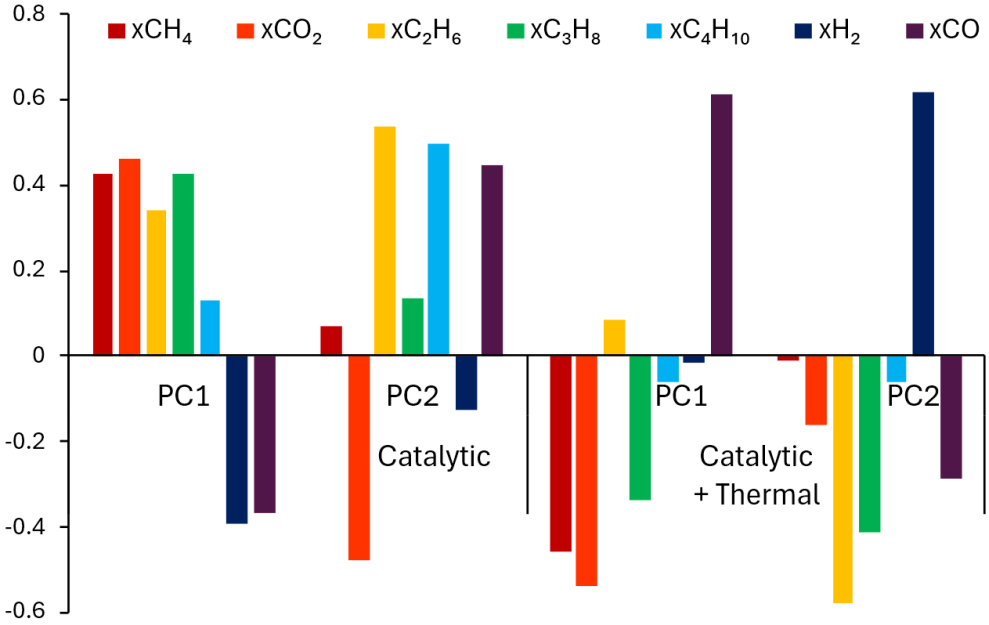

Figure 5. Bar plots of gas loadings for each data group.

Fig. 4), the separation between biomasses and catalyst loadings becomes more defined. For SCB, higher C/B ratios are associated with an upward displacement along PC2, indicating a stronger catalytic influence on yield redistribution. In the case of SAA, samples with lower C/B ratios cluster in the (+PC1, +PC2) region, while higher catalyst loadings shift the samples toward (+PC1, −PC2), with a simultaneous increase along PC2 at the highest C/B values.

Overall, these biplots indicate that the C/B ratio governs the main directions of variance in product yields, but its influence depends strongly on both the biomass type and the reaction regime.

Gas-Phase PCA

Loadings Analysis

The bar plot of the gas-phase PCA loadings (see Fig. 5) reveals a consistent structure between the catalytic

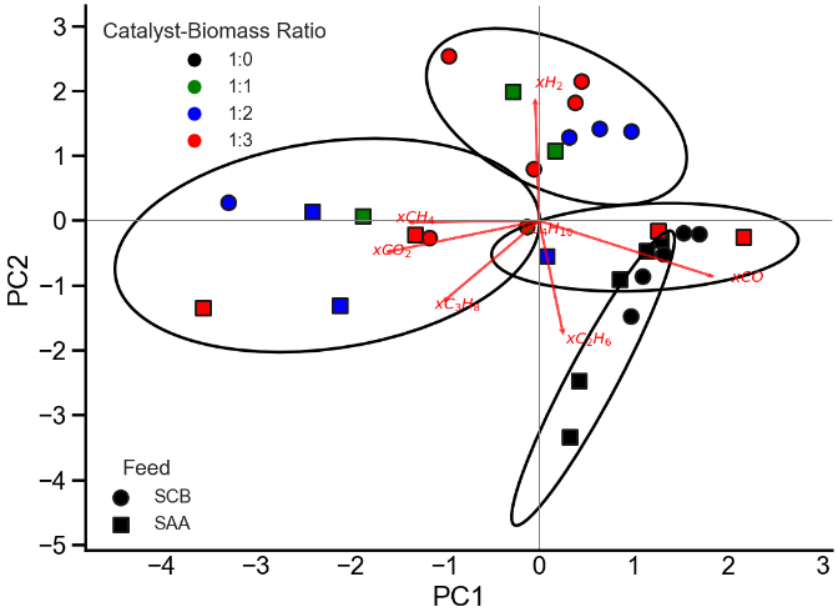

Figure 6. Biplot of thermal + catalytic gas scores.

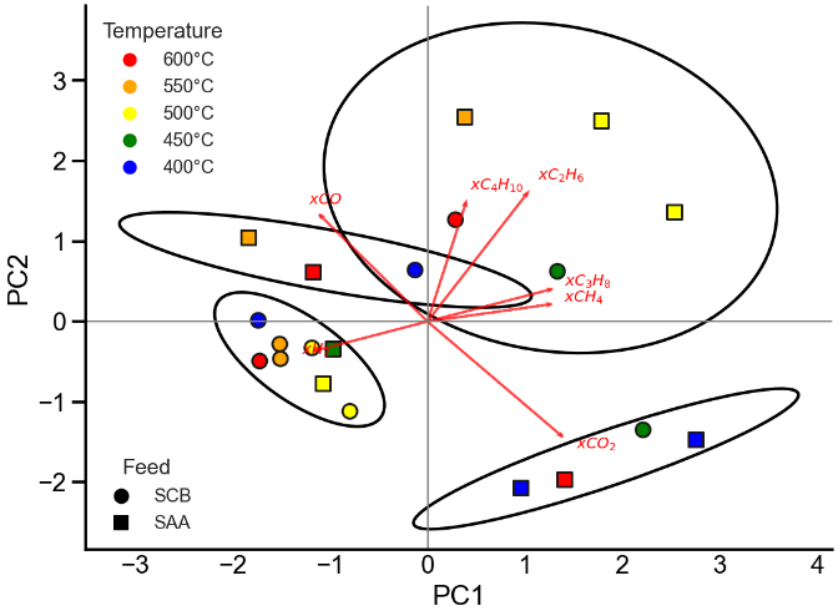

Figure 7. Biplot of only catalytic gas scores.

dataset and the combined catalytic–thermal dataset, indicating that the main gas-forming pathways are intrinsically robust and largely governed by fundamental decomposition and reforming reactions.

In both cases, PC1 is dominated by the major permanent gases, reflecting an axis associated with the extent of gasification and secondary cracking severity. Positive PC1 loadings are linked to increased formation of light gases. This confirms that PC1 represents a global severity coordinate.

PC2 shows a more selective contribution, separating gas species associated with primary thermal devolatilization from those arising from secondary catalytic transformations. In the purely catalytic PCA, PC2 captures subtle shifts in gas selectivity driven by catalyst-assisted pathways, whereas in the combined dataset its relative importance increases, highlighting the growing role of temperature-controlled primary gas release.

The similarity of the loadings pattern indicates that gas-phase composition is less sensitive to the coexistence of thermal and catalytic routes. Instead, gas

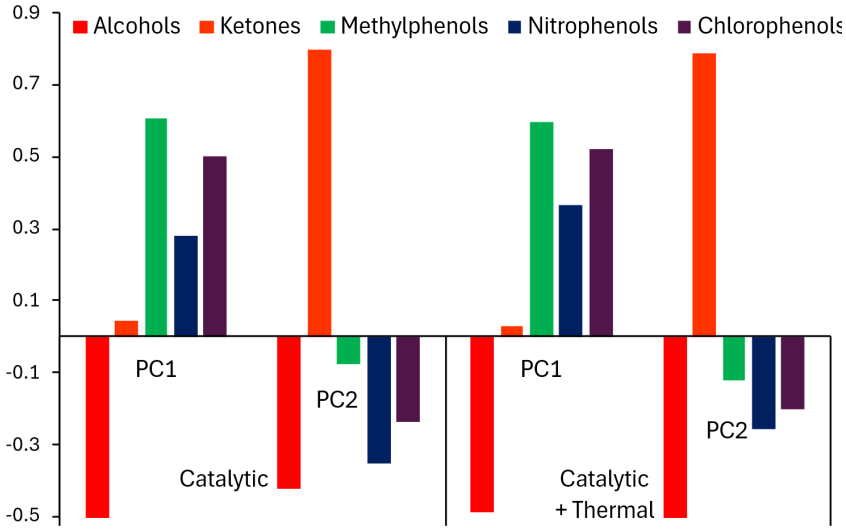

Figure 8. Bar plots of liquid loadings in both groups.

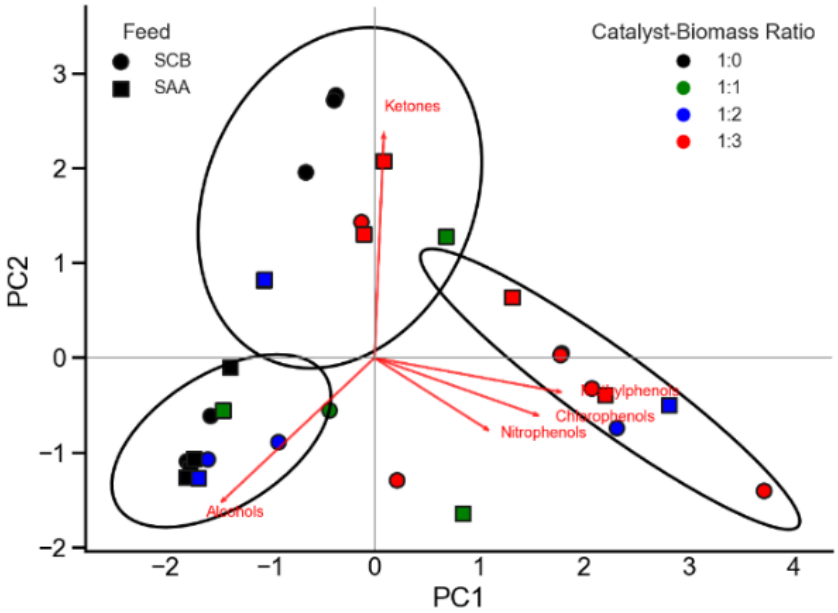

Figure 9. Biplot of thermal + catalytic s liquid scores.

formation responds primarily to the overall intensity of bond scission and reforming reactions, where temperature is the dominant driver and catalyst modulating selectivity.

Biplot Analysis

For the thermo-catalytic dataset, the biplot (see Fig. 6) reveals that thermal experiments are mainly located in the (+PC1, −PC2) region, showing a broader dispersion associated with feedstock type. SCB experiments tend to occupy higher PC2 values, whereas SAA samples are preferentially located at lower PC2 values, indicating distinct gas-phase response patterns between both biomasses under thermal conditions.

In contrast, the catalytic experiments exhibit a clearer organization in terms of the C/B ratio. For SCB, most points are in the (+PC1, +PC2) quadrant, with a systematic upward shift along PC2 as the catalyst loading increases, suggesting an enhanced catalytic contribution to gas-phase transformations. For SAA, although data points remain close to the PC1 axis, an increase in C/B ratio leads to a noticeable displacement toward higher PC1 values, indicating a catalyst-dependent modulation of gas composition.

When considering only catalytic experiments and classifying the data by temperature (see Fig. 7), a strong thermal effect emerges. For SCB, low-temperature experiments cluster in the (+PC1, −PC2) region, while

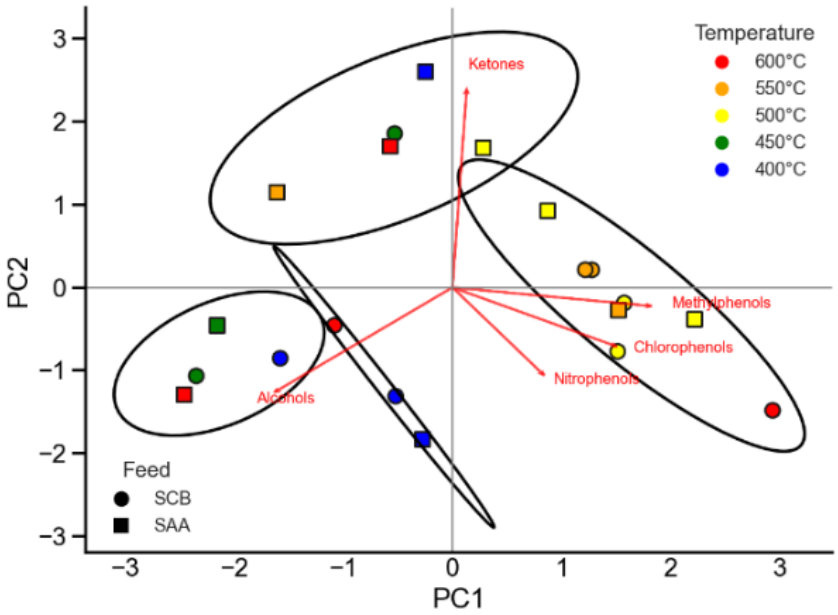

Figure 10. Biplot of only catalytic liquid scores.

increasing temperature drives the data upward along PC2 and progressively toward lower PC1 values. This trend suggests a temperature-driven shift in dominant gas-phase pathways. Conversely, SAA exhibits an opposite behavior along PC2: increasing temperature results in a downward displacement, although a consistent shift toward lower PC1 values is also observed, indicating a shared thermal influence on gas evolution despite biomass-specific differences.

Liquid-Phase PCA

Loadings Analysis

The loadings bar plot for the liquid-phase PCA (see Fig. 8) captures the dominant chemical differentiation within the bio-oil fraction with respect to the first two principal components.

PC1 is primarily governed by the opposition between alcohols and substituted phenolic compounds, defining an axis associated with the structural origin of liquid products. Negative PC1 loadings are dominated by alcohols, which are characteristic of primary depolymerization products from cellulose and hemicellulose. In contrast, positive PC1 loadings are associated with methyl-, chloro-, and nitrophenols, reflecting lignin-derived compounds and secondary aromatic stabilization pathways. This confirms PC1 as a descriptor of increasing aromaticity and secondary processing severity in the liquid phase.

PC2 is strongly controlled by ketones, which exhibit the largest positive loadings in both PCA configurations. This component represents the prevalence of carbonyl-forming fragmentation routes, typically linked to carbohydrate decomposition. Negative PC2 contributions correspond to alcohols and phenolic species, indicating a shift away from simple fragmentation toward more stabilized or condensed liquid products.

When thermal experiments are incorporated, only minor variations in loading magnitudes are observed, while the overall structure of PC1 and PC2 remains unchanged.

This indicates that the chemical partitioning of liquid products is fundamentally preserved, with temperature primarily affecting the distribution of experiments in score space rather than redefining the underlying liquid-phase reaction pathways.

Biplot Analysis

For the thermo-catalytic dataset, the biplot (see Fig. 9) shows that thermal experiments are exclusively located in the negative PC1 region, indicating the absence of liquid-phase stabilization associated with positive PC1 scores.

A clear separation by feedstock is observed along PC2: SCB thermal experiments are mainly located at positive PC2 values, aligned with the ketone-related vector, whereas SAA experiments cluster at negative PC2 values, following the alcohol-related direction.

When analyzing the thermo-catalytic data according to the C/B ratio, most experiments with higher catalyst loading for both biomasses shift toward the (+PC1, −PC2) quadrant. This behavior suggests a catalytic-driven transition toward liquid compositions characterized by enhanced dehydration and secondary transformation pathways.

For the catalytic-only dataset (see Fig. 10), the

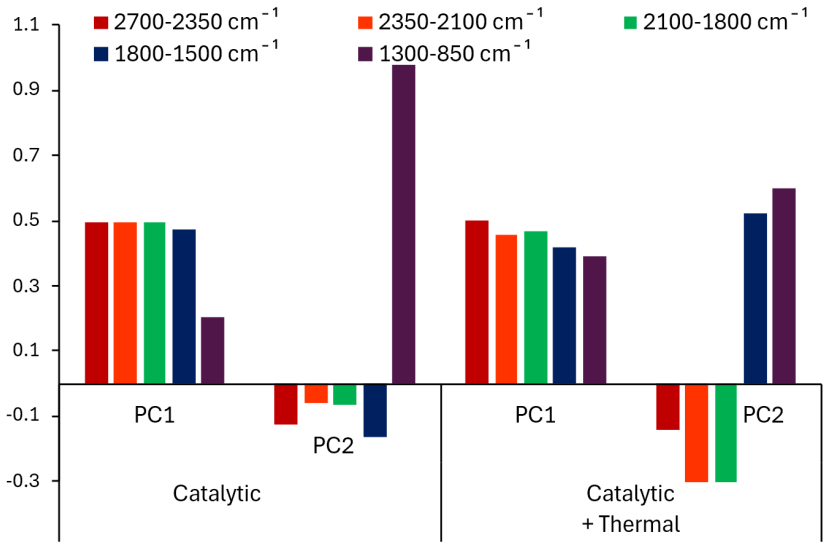

Figure 11. Bar plots, solid FTIR loadings in both groups.

temperature-colored biplot highlights a distinct thermal effect. In SCB, increasing temperature promotes a displacement toward positive PC1 values with intermediate PC2 scores, although all bagasse experiments remain in the negative PC2 region. In contrast, SAA exhibits a different high-temperature response: experiments at 600 °C shift toward lower PC1 values, indicating a tendency toward alcohol- and ketone-rich liquid compositions. Despite these differences, both biomasses show a temperature-dependent reorganization of liquid-phase chemistry under catalytic conditions.

FTIR-Based PCA

Loadings Analysis

The FTIR-based PCA of solid residues (see Fig. 11) exhibits a highly structured behavior, with the first principal component explaining the majority of the variance in both datasets. This confirms that the chemical evolution of the solid phase is governed by a limited number of dominant transformation pathways rather than by random spectral variations.

PC1 is characterized by uniformly positive loadings across all FTIR spectral regions, indicating that it represents the overall intensity and preservation of functional groups in the solid residue. High PC1 values correspond to solids retaining a broad range of oxygenated and aliphatic functionalities, whereas low PC1 values are associated with extensive devolatilization and carbonization, resulting in weak FTIR signals. The slight reduction in PC1 explained variance upon inclusion of thermal experiments suggests the emergence of additional structural diversity in the solid phase at high temperatures.

PC2 provides chemical discrimination among functional groups, separating spectral regions associated with aliphatic and carbohydrate-related vibrations from those linked to more condensed aromatic structures. Positive PC2 loadings are dominated by low-wavenumber regions (1300–850 cm^{-1} and 1800–1500 cm^{-1}), typically attributed to C–O, C–C, and aromatic skeletal vibrations, while negative PC2 contributions are associated with higher-wavenumber regions linked to less condensed structures.

Compared to the catalytic-only PCA, the catalytic–thermal PCA shows a redistribution of PC2 loadings, indicating that temperature enhances structural differentiation within the solid, promoting the coexistence of partially functionalized aromatic char and more condensed carbonaceous domains. Importantly, the interpretation of PC1 as a severity axis and PC2 as a structural-type axis remains robust across both datasets.

Biplots Analysis

For the thermo-catalytic dataset, the biplot (see Fig. 12) reveals a clear and consistent separation between thermal and catalytic regimes along PC1. All thermal experiments are in the negative PC1 region, whereas catalytic experiments shift toward positive PC1 values, indicating the development of more structured and chemically evolved solid residues under catalytic conditions. Along PC2, feedstock-dependent separation is observed: SCB thermal samples are mainly located at negative PC2 values, while SAA samples cluster toward positive PC2.

Within the catalytic experiments, a systematic trend with C/B ratio is evident. For SAA, increasing catalyst loading induces a displacement along a negative slope, with both PC1 and PC2 values decreasing, suggesting progressive modification of surface functionalities and aromatic structures. In contrast, SCB exhibits a more

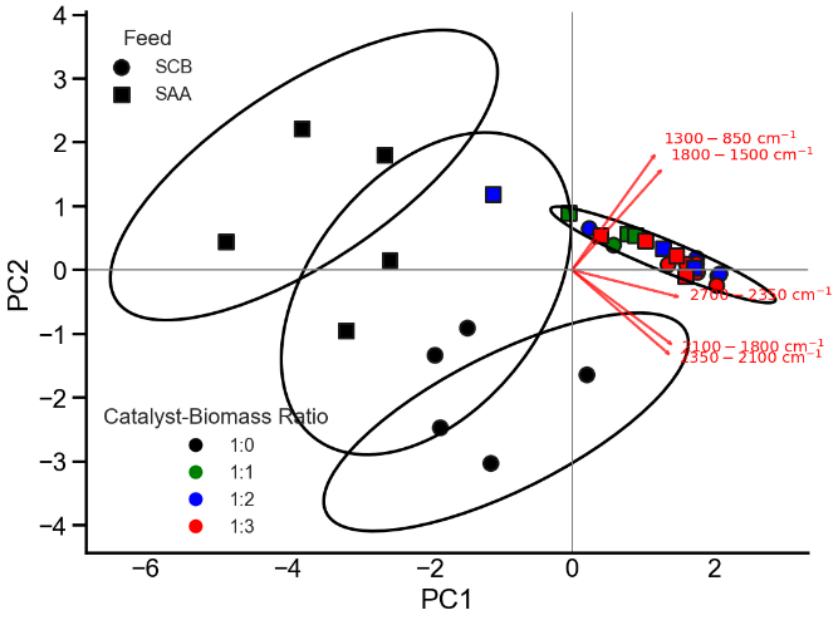

Figure 12. Biplot of thermal+catalytic Solid-FTIR scores.

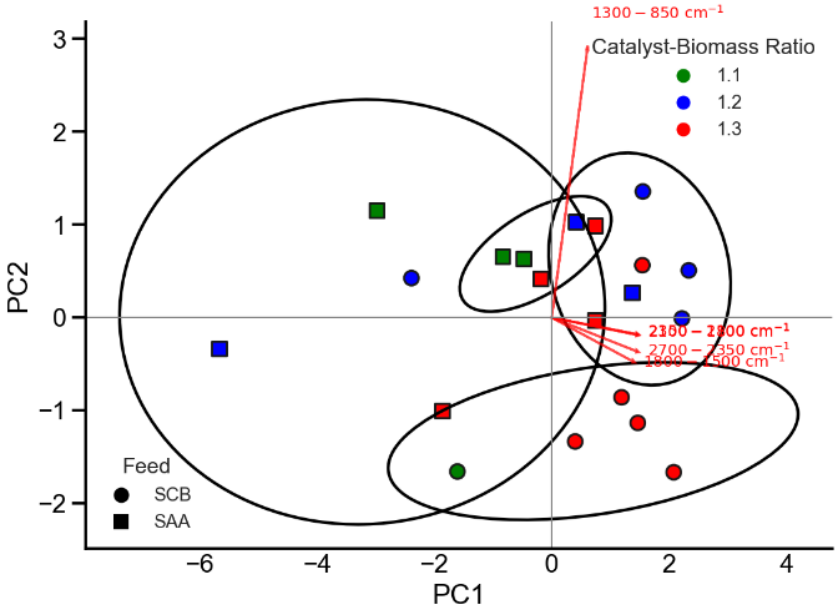

Figure 13. Biplot of only catalytic solid-FTIR scores.

pronounced displacement along PC2, with comparatively minor changes along PC1, indicating a different catalytic restructuring pathway of the solid phase.

For the catalytic-only dataset (see Fig. 13), a distinct feedstock-dependent response is observed. In SAA, increasing C/B ratio promotes a shift toward positive PC1 values, consistent with enhanced catalytic control over char aromatization and functional group evolution. Conversely, SCB samples primarily shift downward along PC2, suggesting progressive loss or transformation of specific surface functionalities rather than changes in overall aromaticity.

Reaction Trends and Proposed Mechanistic Pathways

The integrated interpretation of the PCA results obtained from product yields, gas-phase composition, liquid-phase composition, and solid-phase FTIR provides a

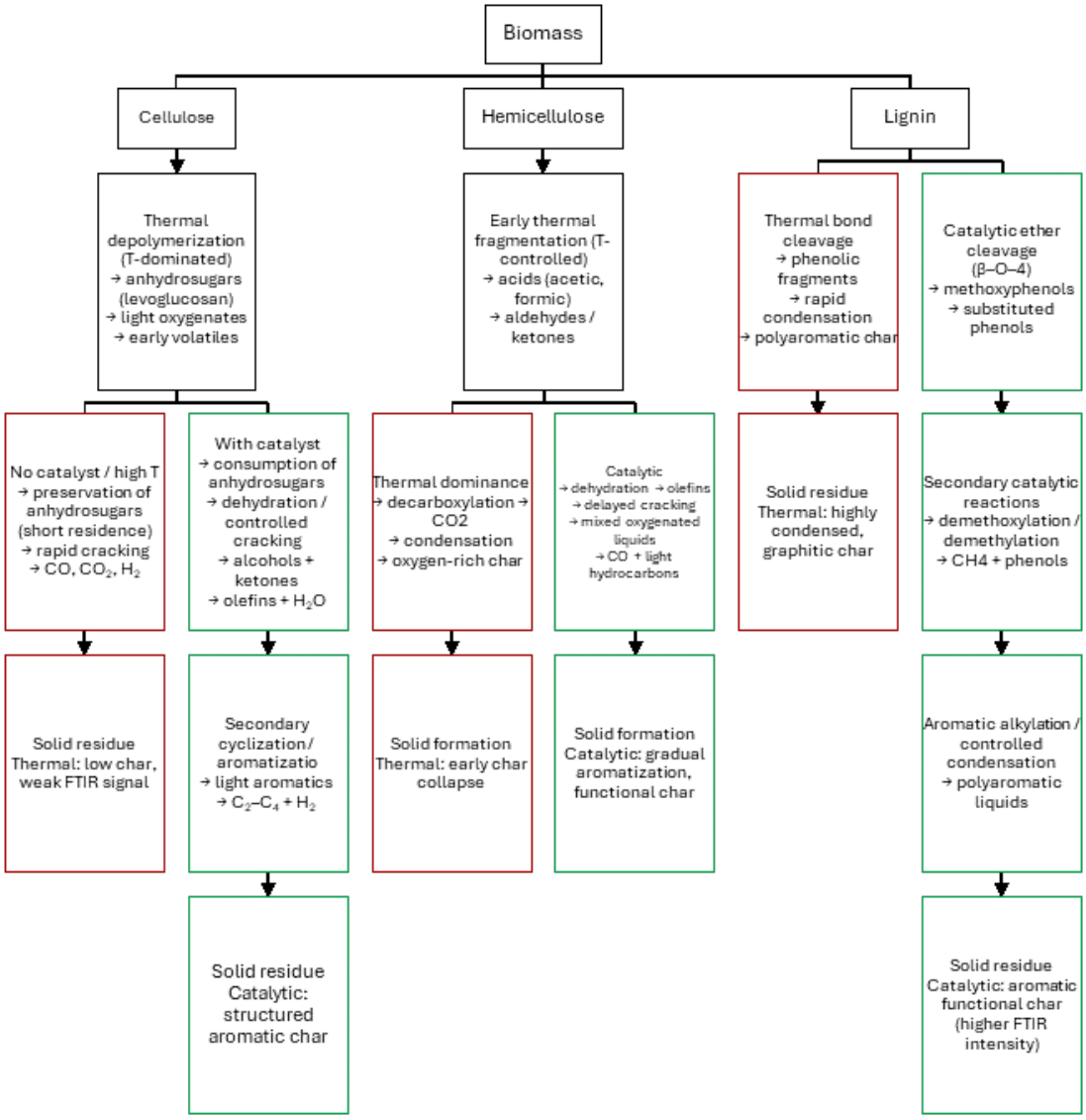

Figure 14: Conceptual reaction scheme for biomass pyrolysis highlighting the main transformation pathways of cellulose, hemicellulose, and lignin into gas, liquid, and solid products of temperature-dominated (red boxes) and catalyst-assisted (green boxes) routes.

consistent basis for proposing the reaction pathways summarized in Fig. 14. The multivariate trends indicate that biomass pyrolysis proceeds through the coexistence of temperature-dominated (red boxes) and catalyst-assisted (green boxes) routes, whose relative contributions depend strongly on feedstock composition.

For SCB, thermal effects primarily govern the initial depolymerization of cellulose and hemicellulose, leading to rapid volatilization and gas formation, as reflected by the clustering of thermal experiments in PCA regions associated with negative PC1 or PC2 values in the yields and gas-phase analyses. As depicted in Fig. 14, the presence of catalyst promotes secondary dehydration, cracking, and aromatization reactions, which are evidenced by systematic displacements along PC1 in yields and gas-phase PCA and along PC2 in FTIR. These trends indicate enhanced formation of light hydrocarbons and aromatics, together with the development of a more structured and aromatic solid residue. The C/B ratio therefore modulates reaction severity and solid-phase restructuring rather than fundamentally altering the primary decomposition pathways of bagasse.

In contrast, SAA exhibits a stronger coupling between catalytic effects and reaction selectivity. The biplots for yields, gases, and liquids show clear and systematic shifts with increasing C/B ratio, particularly along

PC2, indicating a catalyst-driven redistribution among oxygenated liquids, permanent gases, and stabilized solids. This behavior is consistent with the reaction scheme in Fig. 14, where catalytic dehydration, decarboxylation, and controlled condensation pathways become increasingly dominant. The FTIR PCA further supports this interpretation, as catalytic experiments display concurrent displacements along PC1 and PC2, reflecting simultaneous changes in aromaticity and surface functionality of the resulting char.

Overall, the PCA trends across all product phases converge toward a unified mechanistic framework, illustrated in Fig. 14, in which temperature controls primary bond cleavage and volatilization, while the catalyst selectively enhances secondary reactions such as dehydration, decarboxylation, aromatization, and controlled condensation. The balance between these pathways is feedstock-dependent, leading to distinct reaction trends and product distributions for SCB and SAA. This figure-assisted mechanistic interpretation captures the essential reaction behavior inferred from the multivariate analysis without requiring an explicit global PCA.

These observations are also consistent with previously reported descriptions of biomass pyrolysis [1, 8].

CONCLUSIONS

The PCA results demonstrate that separating catalytic and thermal–catalytic datasets is essential to disentangle the dominant reaction regimes during biomass pyrolysis. Temperature primarily governs severe cracking and carbonization pathways, while the catalyst introduces selectivity by promoting secondary reactions and moderating product distribution. The consistent displacement of experimental conditions in the PCA space highlights distinct behaviors for SCB and SAA, linked to their different biochemical compositions. The reaction scheme proposed in this work summarizes these trends and provides a coherent mechanistic framework connecting multivariate patterns with underlying transformation pathways.

ACKNOWLEDGEMENTS

The authors thank the Secretary of Science, Humanities, Technology and Innovation (SECIHTI) of Mexico for the scholarship granted to Martín Rodríguez-Fragoso.

AUTHOR IDENTIFIERS

Author ORCIDs:
Martín Rodríguez-Fragoso: 0009-0003-4299-9641,
Sandro González-Arias: 0000-0002-7395-1566,
Octavio Elizalde-Solis: 0000-0002-7282-3554,
Edgar Ramirez-Jimenez: 0000-0002-3509-0101.

REFERENCES

1. Collard FX, Blin J. A review on pyrolysis of biomass constituents: mechanisms and composition of the products obtained from the conversion of cellulose, hemicelluloses and lignin. Renewable and Sustainable Energy Reviews 38:594-608 (2014). https://doi.org/10.1016/j.rser.2014.06.013
2. Vuppaladadiyam AK, Varsha Vuppaladadiyam SS, Sikarwar VS, Ahmad E, Pant KK, S M, Pandey A, Bhattacharya S, Sarmah A, Leu SY. A critical review on biomass pyrolysis: reaction mechanisms, process modeling and potential challenges. Journal of the Energy Institute 108:101236 (2023). https://doi.org/10.1016/j.joei.2023.101236
3. Wang S, Dai G, Yang H, Luo Z. Lignocellulosic biomass pyrolysis mechanism: a state-of-the-art review. Progress in Energy and Combustion Science 62:33-86 (2017). https://doi.org/10.1016/j.pecs.2017.05.004
4. Aguado R, Elordi G, Arrizabalaga A, Artetxe M, Bilbao J, Olazar M. Principal component analysis for kinetic scheme proposal in the thermal pyrolysis of waste HDPE plastics. Chemical Engineering Journal 254:357-364 (2014). https://doi.org/10.1016/j.cej.2014.05.131
5. Harris CR, Millman KJ, van der Walt SJ, Gommers R, Virtanen P, Cournapeau D, Wieser E, Taylor J, Berg S, Smith NJ, Kern R, Picus M, Hoyer S, van Kerkwijk MH, Brett M, Haldane A, del Río JF, Wiebe M, Peterson P, Gérard-Marchant P, Sheppard K, Reddy T, Weckesser W, Abbasi H, Gohlke C, Oliphant TE. Array programming with numpy. Nature 585:357-362 (2020). https://doi.org/10.1038/s41586-020-2649-2
6. McKinney W. Data structures for statistical computing in python. Proceedings of the Python in Science Conference :56-61 (2010). https://doi.org/10.25080/majora-92bf1922-00a
7. Pedregosa F, Varoquaux, G.Scikit-learn: Machine learning in python. *JMLR* 12:2825-2830 (2011)
8. Ranzi E, Cuoci A, Faravelli T, Frassoldati A, Migliavacca G, Pierucci S, Sommariva S. Chemical kinetics of biomass pyrolysis. Energy Fuels 22:4292-4300 (2008). https://doi.org/10.1021/ef800551t